OBSERVATIONS OF VERTICAL REFLECTIONS FROM THE TOPSIDE MARTIAN IONOSPHERE

E. NIELSEN[1,*], H. ZOU[1,6], D. A. GURNETT[2], D. L. KIRCHNER[2], D. D. MORGAN[2], R. HUFF[2], R. OROSEI[3], A. SAFAEINILI[4], J. J. PLAUT[4] and G. PICARDI[2]

[1]*Max Planck Institute for Solar System Research, 37191 Katlenburg-Lindau, Germany*
[2]*Department of Physics and Astronomy, University of Iowa, Iowa City, IA 52242, USA*
[3]*Istituto di Astrofisica Spaziale e Fisika Cosmica (NAF), 00133 Rome, Italy*
[4]*Jet Propulsion Laboratory, Pasadena, CA 91109, USA*
[5]*Infocom Department, "La Sapienza" University of Rome, 00184 Rome, Italy*
[6]*School of Earth and Space Sciences, Peking University, Beijing 100871, P. R. China*
(*Author for correspondence, E-mail: nielsen@mps.mpg.de)

(Received 30 March 2006; Accepted in final form: 2 November 2006)

Abstract. The Martian ionosphere has for the first time been probed by a low frequency topside radio wave sounder experiment (MARSIS) (Gurnett *et al*., 2005). The density profiles in the Martian ionosphere have for the first time been observed for solar zenith angles less than 48 degrees. The sounder spectrograms typically have a single trace of echoes, which are controlled by reflections from the ionosphere in the direction of nadir. With the local density at the spacecraft derived from the sounder measurements and using the lamination technique the spectrograms are inverted to electron density profiles. The measurements yield electron density profiles from the sub-solar region to past the terminator. The maximum density varies in time with the solar rotation period, indicating control of the densities by solar ionizing radiation. Electron density increases associated with solar flares were observed. The maximum electron density varies with solar zenith angle as predicted by theory. The altitude profile of electron densities between the maximum density and about 170 km altitude is well approximated by a classic Chapman layer. The neutral scale height is close to 10 to 13 km. At altitudes above 180 km the densities deviate from and are larger than inferred by the Chapman layer. At altitudes above the exobase the density decrease was approximated by an exponential function with scale heights between 24 and 65 km. The densities in the top side ionosphere above the exobase tends to be larger than the densities extrapolated from the Chapman layer fitted to the measurements at lower altitudes, implying more efficient upward diffusion above the collision dominated photo equilibrium region.

Keywords: mars, ionosphere, electron densities, top side sounder

1. Introduction

The Earth's upper ionosphere is protected by strong geomagnetic fields from direct interaction with the solar wind. Only at very high latitudes is the ionosphere connected by field aligned currents to interplanetary space. Contrary to this Mars has a rather weak crustal magnetic field over parts of the surface, and the rest of the planet is essentially non-magnetic. The absence of a strong global magnetic field allows the solar wind to directly interact with Mars's upper atmosphere and

Space Science Reviews (2006) 126: 373–388
DOI: 10.1007/s11214-006-9113-y

ionosphere. For strong solar wind pressure a magnetic field may be induced in the ionosphere in order to hold off and deflect the solar wind. The different magnetic characteristics of Earth and Mars lead to significant differences between the top side ionosphere on the planets. The lower ionosphere plasma is expected to be dominated by photo-chemical equilibrium between solar electron/ion production and local losses (Chapman, 1931; Budden, 1966). Apart from solar zenith angle effects, there may be further spatial variations owing to crustal magnetic fields (Nagy *et al*., 2004). However, at higher altitudes, above the photo chemical equilibrium region, vertical diffusion and horizontal plasma transport processes as well as plasma wave activity induced owing to planet rotation, magnetic fields, and solar wind interactions lead to modifications of the plasma at Mars (Luhman *et al*., 1992; Shinagawa, 2000; Acuna *et al*., 1998, 1999; Ness *et al*., 2000; Wang and Nielsen, 2004).

The Martian ionosphere electron densities have been observed before using the radio occultation technique by (Mars 2, 3, 4 and 6, Mariner 4, 6, 7, and) Mariner-9 (Kliore, 1992), by Viking orbiter and Viking landers (Hanson *et al*., 1977), by Mars Global Surveyor (Hinson *et al*., 1999; Bougher *et al*., 2001), and by Mars Express (Paetzold *et al*., 2005). Because Mars is an exterior planet the radio occultation technique allows observations only in a zenith angle range of roughly ± 45 degrees around the terminator. Some results presented in this work are new in the sense that such observations have not been presented before: observations of the Martian ionosphere at small solar zenith angles, direct control of the electron density peak on solar rotation (radiation), and presentation and discussion of virtual and real range obtained by a topside sounder operating at Mars. Other results are new in the sense that we have used a new kind of experiment on Mars and used the measurements to confirm (or dispute) earlier results. Even if we only confirm old results it is worth while to show that the same physics results from different experimental techniques.

MARSIS (= Mars Advanced Radar for Subsurface and Ionosphere Sounding) is a top side sounder, which has been operated on board the ESA spacecraft Mars Express (Nielsen, 2004) since July 2005. The observations are aimed to study the Martian ionosphere and its interaction with the sun (Gurnett *et al*., 2005). The MARSIS experiment is described by Picardi *et al*. (1999).

In this work we demonstrate, that the sounder yields convincing evidence that at the lower altitudes the altitude profile of the electron densities follow the predictions for a Chapman layer, both with respect to zenith angle variations as to control by solar radiation. At higher altitudes the densities are variable and are typically larger than the densities extrapolated from the Chapman layer dominating the densities closer to the density maximum.

2. The Sounder

The radio wave sounder technique has been used extensively to explore the Earth's ionosphere (Budden, 1966; Kenneth, 1965). Sounders have been deployed both on

the ground (Rishbeth and Garriott, 1969) and on orbiting satellites (Nelms *et al.*, 1966). Sounder measurements provide detailed information on variations of the ionospheric electron density with distance from the sounder (Warren, 1963; Hagg, 1967).

Ionosphere soundings rely on the fact that electromagnetic waves can not propagate in a plasma when the wave frequency, f, is below the electron plasma frequency, f_p, and that the wave is reflected where $f = f_p$. The plasma frequency is controlled by the electron density, N_e,

$$f_p^2 = \frac{e^2 N_2}{4\pi^2 m \varepsilon_0} \tag{1}$$

$$f_p = 8.97\sqrt{N_e[\mathrm{el/cm^3}]} \ [\mathrm{kHz}] \tag{2}$$

The basic sounding measurement consists of transmitting a radio wave pulse at a discrete frequency. If the radio frequency is larger than the local plasma frequency the radio wave propagates away from the radar. Specular reflection of the radio signal occurs from regions where the ionosphere is stratified in directions perpendicular to the radar wave vector, and where the plasma frequency (Equation (2)) is equal to the radar wave frequency. The sounder detects the pulse return as a function of time following transmission, the delay time.

The antenna used for transmitting and receiving the radio waves is a dipole, which has a significant gain in all directions (except in directions parallel to the dipole elements). Thus, reflected signals can be received from all directions.

The MARSIS sounder operates with radio waves in the frequency range from 0.1 to 5.4 MHz. This means that electron densities between 125 and 3.8×105 el/cm^3 in the top side ionosphere are probed by the radar. Varying the sounder frequency in steps, a spectrogram of the received signals is build up in a coordinate system of frequency versus delay time. A spectrogram for normal operations displays the intensity of reflected echoes as a function of time for each of 160 discrete frequencies. The time resolution of the measurements is the same as the transmitter pulse width and is 91.4 micros, corresponding to a spatial resolution of $\sim$13.7 km. After transmission of the pulse and a further 162.5 micros dead time, the echo intensity is measured 80 times, covering delay times up to 8 ms or a range of $\sim$1200 km.

3. Single Trace Spectrogram – The Vertical Echo

An example of a spectrogram with a single trace obtained with the top side sounder MARSIS is shown in Figure 1.

This is a typical Martian spectrogram of reflections from the ionosphere in nadir. For this event reflections were observed at frequencies between 1.0 and 3.4 MHz. At low frequencies the echo merges out of background determined by the transmitter power, antenna gain in direction of nadir, and absorption in the ionosphere. The

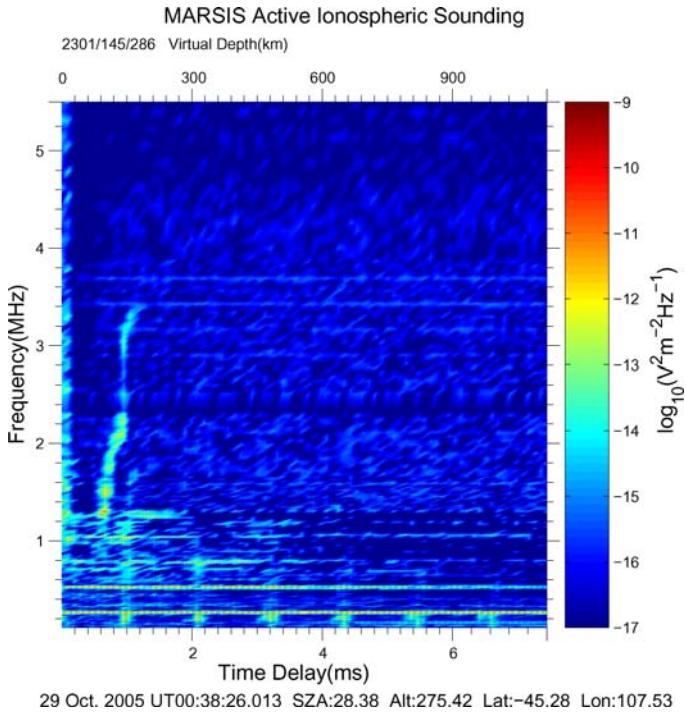

Figure 1. MARSIS spectrogram with frequency versus delay time covering 7.54 ms. The horizontal line near 2.4 MHz is instrumental in origin. A total frequency sweep lasts 1.23 s, and is repeated every 7.5 s.

echoes are reflected at electron densities between 1.24×10^4 and 1.44×10^5 el/cm^3. Delay times are from 0.8 to 1.44 ms. The delay times result from the combined effects of the electron density altitude profile and the altitude of the sounder.

The maximum frequency reflected from the ionosphere is a measure of the maximum plasma frequency (maximum electron density). The maximum plasma frequency may be up to ∼1 MHz on the night side and ∼5 MHz on the dayside.

Since the electron density in the Martian ionosphere is generally decreasing with altitude, low radar frequencies are reflected from the upper parts of the ionosphere, and therefore associated with relatively short delay times. With increasing frequency the reflections occur at larger distances and longer delay times. Radar signals with a frequency exceeding the maximum plasma frequency of the target will penetrate the ionosphere and reach the surface. There it will be reflected/scattered back towards the radar, and if the ionosphere absorption is low enough the ground wave may be detected at the radar (Nielsen *et al.*, 2006). In this particular case no ground wave is observed.

In Figure 1 notice several strong (resonance) horizontal echoes with a separation between nearest neighbors of 265 kHz. These echoes are higher harmonics of the

local plasma frequency at the spacecraft excited by the radar transmissions. The harmonics are caused by nonlinear distortion in the receiver (Gurnett *et al.*, 2006). Using Equation (2) the observed frequency separation translates into a local density of 860 electrons/cm^3. This value of the local density is used later in the inversion process of the spectrograms which yields the vertical electron density profile.

In the following are discussed the maximum electron densities, solar control of the densities, and the altitude profile of the electron densities.

4. The Electron Density Maximum

In connection with ephemeris data the spectrograms yield the density maximum and associated solar zenith angle as they vary during an orbit. We select every 5 minutes the maximum density and zenith angle from all orbits between July and October, 2005. This ensures good coverage in zenith angle and yield a large amount of observations. The Chapman theory predicts that the density maximum (N_m) depends on the sub-solar density (N_0) and zenith angle (θ) as given by Budden (1966)

$$N_m = N_0 \cos^n(\theta) \tag{3}$$

where the simple theoretical value of the exponent is $n = 0.5$. Equation (3) is expected to be valid for zenith angles less than ~85 degrees. Taking the logarithm on both sides a linear least square fit yields $n = 0.48$ and $N_0 = 1.79 \times 105$[el/cm^3],

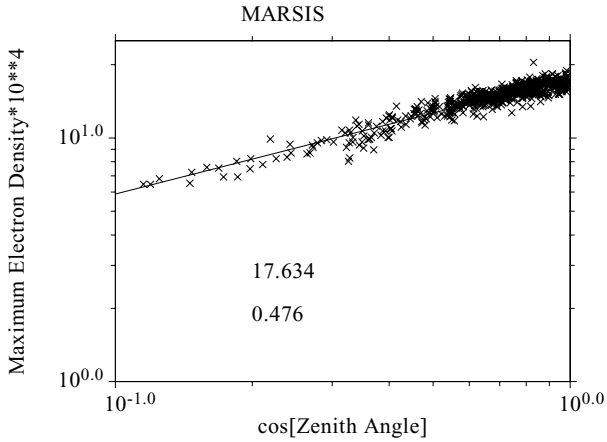

Figure 2. Least squares fit of Equation (3) to observations of maximum density versus zenith angle. For the best fit the exponent is 0.48 consistent with the theoretical prediction, and the maximum sub-solar density is 1.8×10^5 [el/cm^3]. The data are from the latitude interval +75 (north) to −85 degrees.

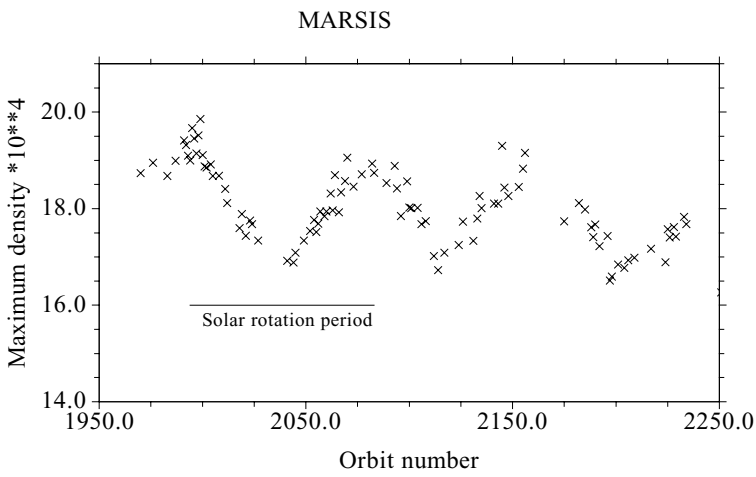

Figure 3. Time variation of the maximum sub-solar electron density (from July 22 to October 14, 2005).

see Figure 2. (This relation is similarly shown to be valid in Figure 3 of Gurnett *et al.* (2005)).

The solid line is the best fit. For zenith angles <85 degree the function sqrt(cos(θ)) is a realistic approximation. For $\theta > 85$ degree ($\cos\theta > 0.1$) the predicted zenith angle dependence require the cos-function in Equation (3) be replaced by the function $1/Ch(x, \theta)$, which takes into account the complications of radiative energy transfer to the atmosphere near the terminator (Chapman, 1931; Rishbeth and Garriott, 1961). The parameter $x = (R_M + h)/H$ is about 350 for Mars ($R_M = 3398$ km, h(height of density maximum) ~130 km, and H(the neutral scale height) ~10 km). Use of the Ch-function improves the fit for large zenith angles. But the function still tends to be a lower limit for densities for zenith angles >90 degrees (Gurnett *et al.*, 2005). Just behind the terminator the electron densities are larger than predicted by photochemical equilibrium. This is likely an effect of transport by winds of dayside plasma across the terminator into the nightside. These results are on line with Zhang *et al.* (1990a,b), Kliore (1992), and Gurnett *et al.* (2005).

It was tested if there were time variations of the electron density taking place during the time interval covered by the observations. For each orbit and for observations with zenith angle $\theta < 85$ degrees the sub-solar density was estimated using Equation (3). Thus, for each orbit the subsolar density was derived for each zenith angle and the average subsolar density calculated. The average of these densities is displayed as a function of orbit number (~time) in Figure 3.

The quite smooth sinusoidal variation of the density with time implies a real time variation of the sub solar densities. That the density variations have a period, which is comparable to the solar rotation period of 26 (Earth-) days points to solar

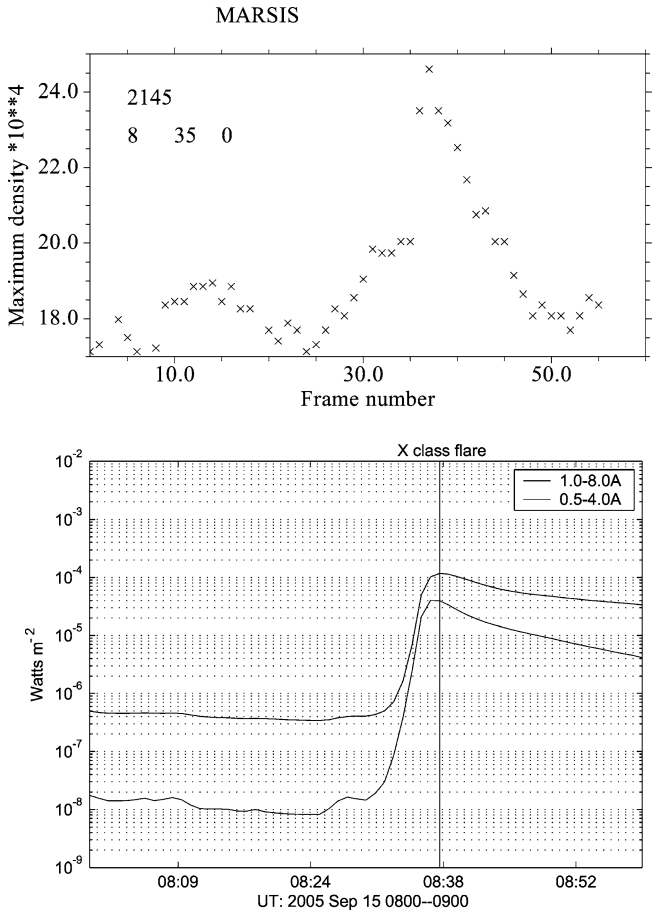

Figure 4. Sudden increase of the electron density maximum (top panel) nearly simultaneous to an increase in solar X-ray flux of wavelength between 0.5 and 3 Angstrom (red curve) and between 1 and 8 Angstrom (blue curve) (bottom panel). The X-ray data are from the GOES spacecraft at the Earth (Bornmann *et al*., 1996). The top panel covers 7 minutes from 0835 to 0842 UT. The bottom panel covers from 0800 to 0900 UT. (All times are on September 15, 2005 (see also Gurnett *et al*. (2005), Figure 3).

radiation as the factor controlling the Chapman layer electron density. This result is consistent with Mendillo *et al*. (2003) and Withers and Mendillo (2005).

During orbit 2145 (September 15, 2005) at ∼0839UT (frame 36 in Figure 4) the electron density maximum in the Martian ionosphere suddenly increased from 1.8×105 to 2.4×105 (Gurnett *et al*., 2005). This coincides closely in time with an increase in solar X-ray fluxes (Bornmann *et al*., 1996) measured onboard GOES spacecraft at the Earth (Figure 4). The X-rays precipitating into the atmosphere are an additional agent of ionization. These X-rays have an ionizing effect at the altitude of the density maximum sufficient to increase the equilibrium maximum electron

density. Similar results on the effects of solar flares on the electron densities were reported recently by Mendillo *et al*. (2006).

5. The Electron Density Altitude Profile

The (typical) echo trace in Figure 1 results from reflections of the sounder waves from horizontally stratified layers of constant electron density in the ionosphere. The trace displays the delay time as a function of sounder frequency.

If the radio waves travelled in vacuum, then the delay time multiplied by the speed of light would equal two times the distance between spacecraft and reflection region. Distances calculated this way are referred to as virtual (or apparent) ranges, r', and have the form,

$$r' = \int_0^{t_d} c dt \tag{4}$$

where c is the speed of light, t_d is delay time, and t is time. However, the radio waves actually propagate through plasma with a group velocity equal to the product of the speed of light and the refractive index of the plasma, n, given by

$$n = \sqrt{1 - \left(\frac{f_p}{f}\right)^2} \tag{5}$$

where n is real for $f > f_p$ (indicating propagation). The group velocity of the radio wave is,

$$v_g = c \cdot n = c \cdot \sqrt{1 - \left(\frac{f_p}{f}\right)^2} < c \tag{6}$$

Since f_p^2 is proportional to the electron density the speed with which the radio wave propagates is a function of the local electron density. The real distance travelled by the radio wave in time t_d is

$$r = \int_0^{t_d} cndt \tag{7}$$

Rewriting this equation we have an expression for the delay time,

$$t_d = \int dt = \int \frac{dr}{c \cdot n} \tag{8}$$

the integral is along the round trip, radar-reflection-radar.

For each signal frequency the observed delay time multiplied by the speed of light and divided by two is the virtual range to the reflection region where the plasma frequency equals the signal frequency. The virtual ranges depend on the spatial variations of the electron density between the spacecraft and the reflection

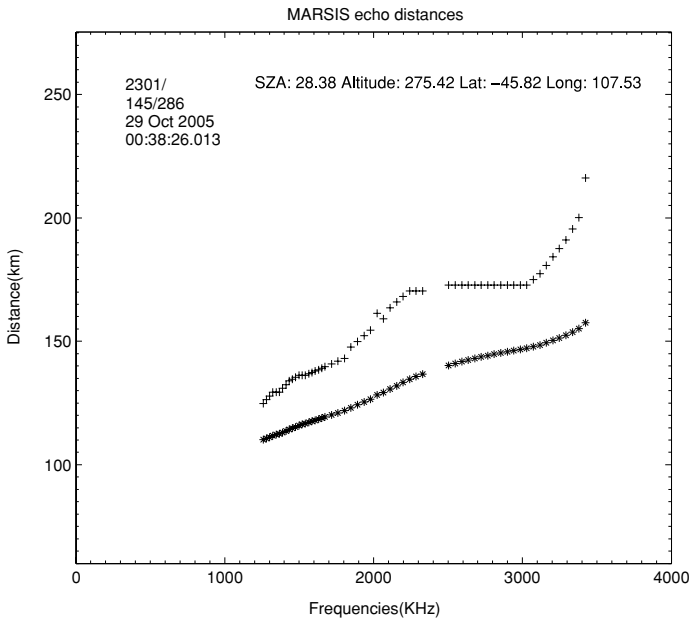

Figure 5. The upper curve is derived from the data in Figure 1 by multiplying the observed delay times with the speed of light (virtual range). This curve is known as an ionogram. The lower curve is the real range variations derived using the lamination technique (see text).

region. Since the propagation speed is reduced in the plasma the virtual range is an upper limit on the real range.

The echo trace in Figure 1 was digitized and the virtual ranges (or distances) versus the sounder frequencies are shown by the upper curve in Figure 5. The top-side sounder measurements cover that part of the ionosphere located below the spacecraft and higher than the altitude of the maximum plasma frequency. For this case the virtual distances vary from ∼110 to 160 km. In this case the virtual distance increases with frequency in the whole interval. However, note that for some events the slope of the curve for the lower frequencies is negative, i.e. the virtual distance decreases with increasing frequency. If the distances were real this would not be physically possible; because it implies that lower electron densities are observed at larger distance than higher density layers. However the distances shown are virtual distances. In order to reduce the virtual distances to realistic real distances one must take into account the densities between the spacecraft and the region of reflection of the lower frequencies.

The next step is to invert the observed virtual ranges into a self consistent real electron density profile, with real ranges, such that Equation (8) is satisfied.

The ionogram can be inverted to a real height profile of electron densities using the lamination technique (see Zou and Nielsen, 2004). In this method the ionosphere between the spacecraft down to the maximum electron density is divided into a series

of horizontal slabs (N), and it is assumed that the real range varies linearly with plasma frequency inside a slab such that dr/df = constant. For distances closer to the spacecraft than the distance to the lowest frequency reflection point the electron density is assumed to decrease exponentially with altitude with a scale height H_t.

The variable 'time' (in Equation (4)) is replaced by the variable 'real range', or distance. Using that $dt = dr/cn$ and that dr/df is constant within each slab, Equation (4) is modified to

$$r' = \int_0^{t_d} \frac{1}{n} \int_{f_0}^{f_{\max}} \frac{1}{n} \frac{dr}{df} \int_{f_0}^{f_{\max}} \frac{1}{n} df \tag{9}$$

where f_0 is the plasma frequency at the spacecraft and $f_{\max}$ is the plasma frequency at the maximum electron density. This form of the virtual height equation reveals that the virtual range rapidly increases where the curve r' versus f' is steep (dr/df large). This is the case near the peak of a density layer, as for example near the maximum plasma frequency. As noted above this effect can be seen in Figure 1.

Writing this equation for each of the slabs starting from the top ($i = 0$) to slab $i = j$ and summing over range, we have,

$$r' = \sum_i^j dr_i \left(\frac{1}{df_{i,i-1}} \int_{f_{i-1}}^{f_i} \frac{1}{n} df \right) = \sum_i^j dr_i M(j,i) \tag{10}$$

Here are N equations with N unknown real range intervals, dr_j, one for each slab. Recognizing that M is a matrix the set of equations can be inverted and solved for dr,

$$dr = M^{-1} r' \tag{11}$$

and finally the real range to slab j is,

$$r_j = \sum_{i=1}^{j} dr_i \tag{12}$$

First some general comments to the inversion process. If echoes were observed all the way from the spacecraft to the density maximum the inversion could be carried out self consistently. In this case the first slab is at the spacecraft and the N'th slab at the distance to reflection of the highest observed frequency. However, typically the range to the first reflection point is not zero but a considerable distance from the spacecraft. The densities within this distance are not known. In order to proceed with the inversion one must make an assumption about these densities.

We have carried out the inversion using the local density at the spacecraft derived from the plasma frequency oscillations as an 'anchor point'. We use the earlier determined density at the spacecraft and assume the density variation between the spacecraft and the first reflection point is exponential with a scale height H_t (which

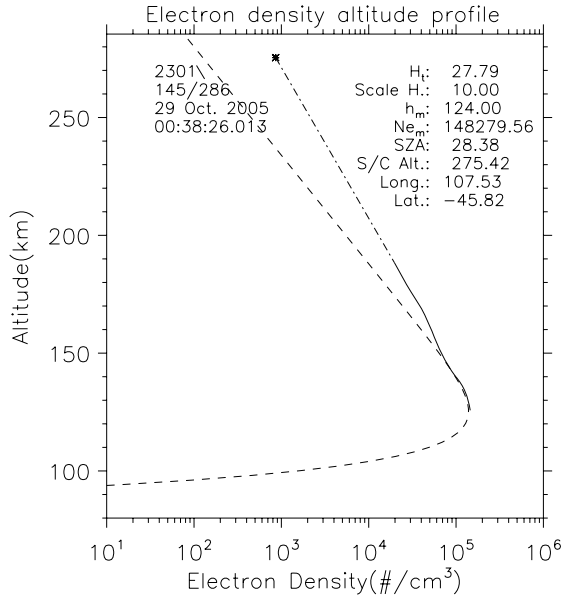

Figure 6. The solid and dash-dot curve is the estimated profile of the top side electron densities derived using the lamination technique. The solid curve covers the densities for which echoes were observed, and the dash-dot curve the assumed exponential decrease. Note, the dash-dot curve starts at the derived electron density (star) at the height of the spacecraft. The dashed curve is a Chapman layer fitted to the observations. In the plot is noted the associated maximum electron density (148279 el/cm^3) and altitude of the maximum (∼124 km) in the sub solar region, together with the neutral scale height (10.0 km), a top-side scale height (∼28 km), and solar zenith angle (∼28 degrees).

is determined by the analysis). This approach is only possible when the plasma frequency can be determined from the observations. That is not always possible.

This approach is only valid within the assumption of exponential decay. The actual profile may be non-exponential. If the profile is non-exponential that will influence the derived distance and densities between spacecraft and the first point of reflection. There seems to be a trend in the data that an exponential decay is a good first approximation but not a complete description. If the assumed exponential decrease is overestimating/under estimating the densities then the derived real distance from spacecraft to first reflection point will be an underestimate/overestimate, and the altitude of the density maximum will be overestimated/underestimated.

The inversion technique has been applied to the data in Figure 1 and Figure 5. Figure 5 also displays the derived real range curve (the lower curve). With the spacecraft height this real range curve has been transformed to the height versus electron density curve, solid in Figure 6. The exponential decrease (dash-dot curve) of electron densities at high altitudes (with $H_t \sim 28$ km) is also included in the figure; the curve starts at the altitude of the spacecraft at the observed local electron density (marked by a star).

Next we test how the real density profile fits to the predictions of the Chapman theory. The electron density profile in a Chapman layer is given by,

$$N_e(h) = N_o \exp \frac{1}{2}\left[1 - \frac{h - h_o}{H_1} - \sec(\theta) \exp\left(-\frac{h - h_0}{H_1}\right)\right] \tag{13}$$

where h_o is the sub solar maximum electron density and altitude of the density maximum. θ is the solar zenith angle. H_1 is the neutral atmosphere scale height. For a scale height of 10 km the layer is a good fit to the observed density profile. The predicted profile for a zenith angle of 28 degrees is displayed in Figure 6 (dashed). Clearly the observations and theory matches very well for altitudes around the electron density maximum up to an altitude of 160 km. The scale height is in the range determined in earlier Martian electron density measurements. It is concluded that up to an altitude of ∼160 km, the observations are well represented by a Chapman layer.

To check the derivations we have used the derived real profile curve for all altitudes above the density peak to calculate the delay time versus frequency. We

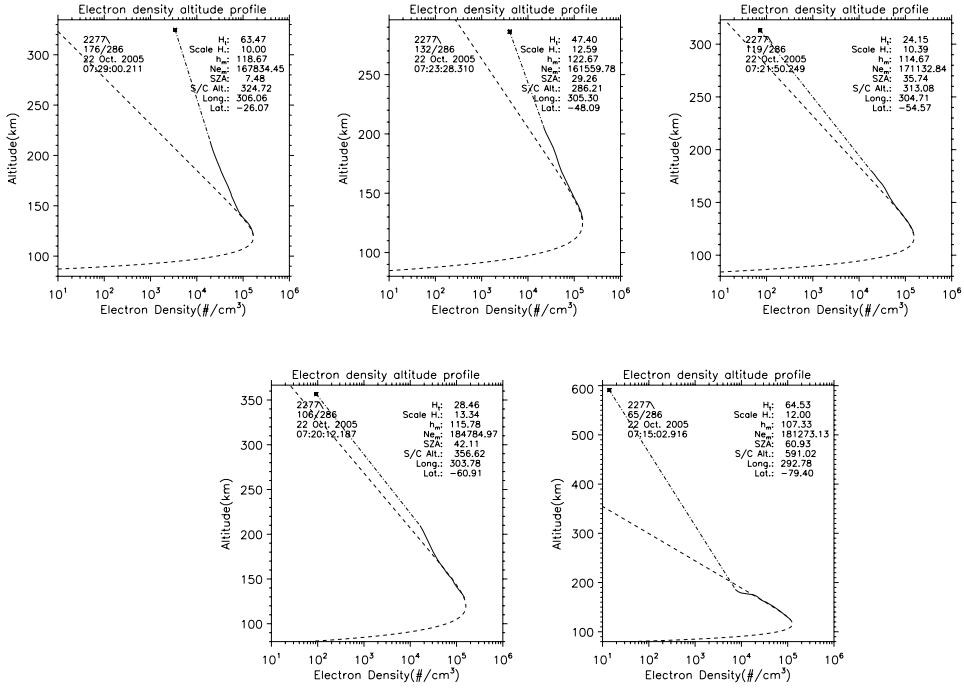

Figure 7. Five electron density profiles from the same orbit (2277) for solar zenith angles between ∼7 and 60 degree, with fitted Chapman functions. Increased diffusion above ∼180 km leads to densities which are relatively high when compared to the Chapman layer fitted to the observations at lower heights.

find the predicted time delays are in good agreement with the observed ones. This implies self consistency of the inversion process.

In Figure 7 are shown 5 panels with electron density profiles derived as described above in the solar zenith angle interval from 7 to 60 degrees. In all cases there is a good fit of the data to a Chapman layer from the density maximum up to about 160 km. The neutral scale height is from 10 to 13 km. At higher altitudes the scale height increases to values between 24 and 65 km. Thus the density in the top side ionosphere exceeds the densities in the Chapman layer extrapolated above 160 to 180 km. With decreasing collisions the plasma is apparently able to more effectively diffuse upward above 180 km.

It is concluded that the ionosphere at the density peak and in the altitudes above up to $\sim$180 km is well described as a Chapman layer with a neutral scale height from 10 to 13 km. This means that the photochemical equilibrium region extends up to between 160 and 180 km in good agreement with earlier results. Above the equilibrium region the scale height is between 24 and 65 km also in the same framework as earlier results.

The measurements were obtained with a top side sounder radar, a new instrument of a kind not flown before at Mars. The measurements extend for the first time to zenith angles less than 48 degrees. Examples of MARSIS spectrograms have illustrated several points about the day side Martian ionosphere:

1. the zenith angle dependence of the electron density maximum is as predicted by the Chapman theory. This was shown in a statistical sense, in Figure 2;
2. the density maximum is controlled by solar radiation and varying with solar rotation;
3. solar flare X-ray burst causes increase of the electron density maximum;
4. the electron density altitude profile just above the density peak is well described by a Chapman function with a neutral atmosphere scale heights between 10 and 13 km,
5. the ionosphere above the photoequilibrium region, ending at between 160 and 180 km, is variable and was approximated by an exponential decrease corresponding to minimum scale heights between 24 and 65 km.

These results were partly reached by analyzing the echoes reflected from the ionosphere in the nadir using the lamination method to invert the observed ionograms.

6. Discussion

A top side ionospheric sounder measures the delay times for radio waves propagating from the sounder to a reflection region and back, as a function of frequency. MARSIS measures electron densities in the range from 125 to 3.8×10^5 el/cm^3. The sounder transmit in a broad angular interval (essentially 4π) centered on the

nadir. Specular reflections occur from the Fresnel zone which has a dimension of 23 km at a frequency of 2 MHz and a spacecraft altitude of 900 km. Altitude variations in the reflections over the Fresnel zone would tend to widen the spectrogram trace. Occasionally the width of the echo trace corresponds to a range interval of $\sim$30 km indicating simultaneous reflections can occur in neighboring range bins.

Provided observations are available all the way from the spacecraft to the reflection point, Equation (10) can be inverted to yield the electron density as a function of radar range (or of height above the planet surface). However, normally the closest echo originates some distance from the sounder. Since the radio waves are also influenced by the electron densities in the 'blind region' between the spacecraft and the first echo, one must in order to proceed assume how the density varies in that region. The local density at the spacecraft can often be derived from resonance lines in the spectrogram. They occur with a separation between neighboring lines at the plasma frequency of the local plasma. The density profile in the blind region is assumed to start with the local density at the spacecraft altitude and to be exponentially decreasing with altitude below the spacecraft. This assumption allows the data to be inverted to yield the real electron density profile using the lamination technique.

In this report MARSIS observations between 7 and 60 degree solar zenith angle are presented.

The ionosphere is typically characterized by a spectrogram with a single trace of reflections. For each frequency there is only a reflection for one delay time. This implies a horizontally stratified ionosphere with an electron density gradient pointing towards the sounder.

The maximum plasma frequency corresponds typically to a maximum density in the range 10^4 to 10^5 el/cm^3, values consistent with earlier results. The solar zenith angle dependence of the density maximum is as predicted by theory: the density decreases as the square root of the cosine to the zenith angle (Equation (3)) for angles $<$85 degree and as the square root of the inverse Chapman function for angles $>$85 degree.

The density maximum is varying periodically in time with the solar rotation period implying that solar radiation controls the maximum. X-rays are known to cause excess ionization in the Earth's ionosphere, giving rise to Sudden Cosmic Noise Absorption. X-ray bursts were found to coincide with a density increase also in the Martian ionosphere. Such an effect of solar X-rays on Mars has been suggested in the past (Nielsen, 1998).

The observations further confirm that the density profile from the maximum and up to an altitude of 160 to 180 km is well described as a Chapman layer. The equivalent subsolar altitudes of the electron density maximum is from 107 to 123 km. The neutral air scale height in the Chapman layer varied between 10 and 13 km. At higher altitudes the density decreased exponentially with a scale height in the range 24 to 65 km. These parameter values are in general agreement with earlier results. Note that the altitude of the density maximum is dependent on the

assumed exponential decrease of the densities in the 'blind region'. Deviations from the assumption could raise or lower the altitude of the density maximum. The assumption has however little influence on the values of the other parameters characterizing the Chapman layer.

Note, that these results are also valid for zenith angles <48 degree. This is outside the zenith angle range accessible to previous measurements.

Acknowledgements

MARSIS was built and is jointly managed by the Italian Space Agency and NASA. Mars Express was built and is operated by the European Space Agency. The research at the University of Iowa was supported by NASA through contract 1224107 with the Jet Propulsion Laboratory.

References

Acuna, M. H., Connerney, J. E. P., Ness, N. F., Lin, R. P., Mitchell, D., *et al.*: 1999, *Science* **284**, 790.

Acuna, M. H., Connerney, J. E. P., Wasilevsky, P., Lin, R. P., Anderson, K. A., Carlson, C. W., *et al.*: 1998, *Science* **279**, 1676.

Bornmann, P. L., Speich, D., Hirman, J., Mathison, L., Grubb, R., Garcia, H., *et al.*: 1996, *Proc. SPIE* **2812**, 291.

Bougher, S. W., Engel, S., Hinson, D. P., and Forbes, J. M.: 2001, *Geophys. Res. Lett.* **28**, 3091.

Budden, K. G.: 1966, *Radio Waves in the Ionosphere*, The University Press, Cambridge.

Chapman, S.: 1931, *Proc. Phys. Soc.* **43**, 483.

Gurnett, D. A., Huff, R. L., Morgan, D. D., Persoon, A. M., Averkamp, T. F., Kirchner, D. L., *et al.*: 2006, COSPAR.

Gurnett, D. A., Kirchner, D. L., Huff, R. L., Morgan, D. D., Persoon, A. M., Averkamp, T. F., *et al.*: 2005, *Science* **310**, 1929, 10.1126/science.1121868.

Hagg, E. L.: 1967, *Can. J. Phys.* **45**, 27.

Hanson, W. B., Sanatani, S., and Zuccaro, D. R.: 1977, *J. Geophys. Res.* **82**, 4351.

Hinson, D. P., Simpson, R. A., Twicke, J. D., Tyler, G. L., and Flasar, F. M.: 1999, *J. Geophys. Res.* **104**, 26997.

Kenneth, D.: 1965, *National Bureau of Standards Monograph* **80**.

Kliore, A. J.: 1992, In *Venus and Mars: Atmospheres, Ionospheres, and Solar Wind Interactions*, Geophysical Monograph 66, American Geophysical Union.

Luhmann, J. G., Tatrallyay, M., and Pepin, R. O.: 1992, in Luhmann, J. G., Tatrallyay, M., and Pepin, R. O. (eds.), *Geophysical Monograph* 66, American Geophysical Union.

Mendillo, M., Smith, S., Wroten, J., Rishbeth, H., and Hinson, D.: 2003, *J. Geophys. Res.* **108**(A12), 1432, doi:10.1029/2003JA009961.

Mendillo, M., Withers, P., Hinson, D., Rishbeth, H., and Reinisch, B.: 2006, *Science* **311**, 1135.

Nagy, A. F., Winterhalter, D., Sauer, K., Cravens, T. E., Brecht, S., Mazelle, C., *et al.*: 2004, *Space Sci. Rev.* **111**, 33.

Nelms, G. L., Barrington, R. E., Belrose, J. S., Hartz, T. R., McDiarmid, I. B., and Brace, L. H.: 1966, *Can. J. Phys.* **44**, 1419.

Ness, N. F., Acuna, M. H., Connerney, J. E. OP., Kliore, A. J., Breus, T. K., Krymskii, A. M., *et al.*: 2000, *J. Geophys. Res.* **105**, 15991.

Nielsen, E., Morgan, D. D., Kirchner, D. L., Plaut, J., and Picardi, G.: 2006, *Plan. Space Sci.*, in press.
Nielsen, E.: 2004, *Space Sci. Rev.* **111**, 245.
Nielsen, E.: 1998, in Attema, E., Schwehm, G., and Wilson, A. (eds.), *Proc. 32nd ESLAB Symp. 'Remote Sensing Methodology for Earth Observation and Planetary Exploration' ESTEC,* Noordwijk, *The* Netherlands, ESA SP-423, ESA Publ. Div., Noordwijk, pp. 215–223.
Pätzold, M., Tellmann, S., Häusler, B., Hinson, D., Schaa, R., and Tyler, G. L.: 2005, *Science* **310**, 837.
Picardi, G., Sorge, S., Seu, R., Fedele, G., Federico, C., and Orosei, R.: 1999, Mars advanced radar for subsurface and ionosphere sounding (MARSIS). Info-Com. Dept., Technical report N. MRS-001/005/99, version 2.0.
Rishbeth, H., and Garriott, O. K.: 1969, *Introduction to Ionospheric Physics*. International Physics Series, Volume 14, Academic Press.
Shinagawa, H.: 2000, *Adv. Space Res.* **26**(10), 1599.
Shinagawa, H., and Cravens, T. E.: 1989, *J. Geophys. Res.* **94**(A6), 6506.
Wang, J.-S., and Nielsen, E.: 2004, *Ann. Geophysicae* **22**(1–5), SRef-ID: 1432-0576/ag/2004-22-1.
Warren, E. S.: 1963, *Nature* **197**, 636.
Withers, P., and Mendillo, M.: 2005, *Planet. Space Sci.* **53**, 1401.
Zhang, M. H. G., Luhmann, J. G., Kliore, A. J., and Kim, J.: 1990a, *J. Geophys. Res.* **95**(B9), 14829.
Zhang, M. H. G., Luhmann, J. G., and Kliore, A. J.: 1990b, *J. Geophys. Res.* **95**(A10), 17095.
Zou, H., and Nielsen, E.: 2004, Methods for obtaining electron density profiles from MARSIS ionograms and derivation of parameters characterizing the profiles. MPAe-W-485-04-01.